Inspection Techniques Using Scanning Acoustic Microscopy for Silver Sintering Applications in Power Electronic Modules

Heaklig Ayala
School of Engineering
University of Warwick
Coventry, United Kingdom
0000-0001-9828-7289

Jose Ortiz Gonzalez
School of Engineering
University of Warwick
Coventry, United Kingdom
J.A.Ortiz-Gonzalez@warwick.ac.uk

Mohammed-Amer Karout
School of Engineering
University of Warwick
Coventry, United Kingdom
0000-0003-1660-1196

James Cotty
Automotive EV
Custom Interconnect Limited
Andover, United Kingdom
James.Cotty@cil-uk.co.uk

Tim Rumney
Automotive EV
Custom Interconnect Limited
Andover, United Kingdom
Tim.Rumney@cil-uk.co.uk

Philip Mawby
School of Engineering
University of Warwick
Coventry, United Kingdom
P.A.Mawby@warwick.ac.uk

***Abstract*— This work presents a practical perspective to Scanning Acoustic Microscopy (SAM) for Ag-sintering applications in power electronic modules and devices. It aims to present typical challenges to consider whilst performing C-SAM for inspecting and analysing microstructures within power electronic devices, with emphasis on silver-sintered interconnects. The study presents a vast number of acoustic images (discrete devices in TO-247 packages, power modules, and also custom samples of substrates and devices), where several defects are identified, including voids, cracks, and delamination. Challenges for Ag-sintered layers inspection related to advanced surface finishes are also revealed and discussed in detail. The suitability of C-SAM for inspecting small and large areas of Ag-sintered interfaces is discussed, and showcased with custom samples, and a commercial power module.**

Keywords*— *SAM, C-SAM, Sintering, Ag-Sintering, Power Modules

I. Introduction

Ag-sinter technology has proven to be most favourable for power electronic applications requiring high operating temperatures and power cycling, meaning it is a good candidate for power module packages containing wide-bandgap semiconductors [1]. Nevertheless, there are challenges regarding the inspection techniques of Ag-sintered layers, which arise from recent advanced substrate metallisation types, dispensing and curing techniques, and the relatively small thicknesses of Ag-layers compared to the neighbouring structures, just to mention a few. Scanning Acoustic Microscopy (SAM) is an adequate non-destructive inspection technique, that allows to efficiently spot defects such as cracks, voids, and delamination [2]. Therefore, proper inspection by means of SAM can allow to further optimise assembly processes.

The process of Ag-sintering is sensitive to various process parameters such as pressure, temperature, or even different process atmospheres. In order to achieve a reliable attach, the condition of the mating surfaces and the sinter paste also plays an important role [1].

Because the imaging technique is purely based on physical interactions of ultrasound waveforms with mechanical structures, the technique can efficiently find physical defects which would be very hard (sometimes impossible) to identify otherwise. For instance, adhesion problems can occur during sintering due to multiple reasons (e.g., contamination), but they cannot be detected properly using X-Ray. SAM can prove particularly important during process monitoring during specific production stages, because not all the issues during assembly can be identified simply with an end-of-line electrical test [1].

So far, X-Ray is the de facto imaging technology in semiconductor industry. Here, an image contrast is achieved because of the absorption of X-Rays in the sample, meaning this transmission imaging technique can only provide volume information of the defects, and is not as effective for the detection of interface defects (e.g., delamination), or even adhesion problems [1]. Unlike X-Ray, inspection of interfaces is the area where SAM excels in particular compared to other methods, especially in the context of power electronics.

Bringing another technology into the equation, SAM could also be compared to thermography methods. Both SAM and thermography are more sensitive to interface defects compared to X-Ray. However, even though SAM can provide higher resolutions compared to thermography, the sample has to use a water coupling medium [1], which can make it less attractive as it is normally achieved by submerging the sample into the fluid.

A scanning acoustic microscope (SAM) emits an ultrasonic beam onto the specimen, such as the structure of a semiconductor package, and then converts the reflected "echo" intensity at the boundary between different materials into gradient values. The transducer accomplishes the task of sending an ultrasonic signal that hits the sample, which is then received through reflection of the same signal as it hits different interfaces (because of acoustic impedance

This work has been supported by the Centre for Doctoral Training (CDT) to Advance the Deployment of Future Mobility Technologies at the University of Warwick, Coventry, UK. The studentship is partially supported by Custom Interconnect Ltd. (Group), Andover, UK.

mismatch). Finally, the signals received are used for imaging and defect detection [3].

The acoustic impedance (Z) can be defined as the resistance a material poses to the propagation of an ultrasound beam as it penetrates through it:

$$Z = \rho \times c \tag{1}$$

Where: ρ is the material density (in $\mathrm{kg/m^3}$); c is the velocity of sound within the material (in $\mathrm{m/s}$); and Z is related to the acoustic hardness of the material (in $\mathrm{Ns/m^3}$).

Examples of acoustic impedance related properties are provided in TABLE I.

Reflection and scattering happen at the different interfaces of the sample, which depend greatly on the geometry of the defect and the materials involved. The proportion of the reflected waves compared to the transmitted ones is determined from the impedance mismatch of the materials involved. A higher acoustic impedance mismatch at the interface would imply a larger intensity of the reflection [2].

The reflected ultrasound is received using a transducer which then converts it into an electronic signal [4]. The reflection index then given by:

$$R = \frac{(Z_2 - Z_1)^2}{(Z_2 + Z_1)^2} \tag{2}$$

Similarly, the transmission index can be simplified as:

$$T = 1 - R \tag{3}$$

The role of the transducer is very important, and as the "lens", its geometry optimises for proper focus on the area of interest, as well as for resolution, and penetration depth [2]. The ultrasonic pulse generated from the transducer is delivered to the sample via a water coupling medium, since air reflects practically all the ultrasound due to its characteristic acoustic impedance.

During the process of sending the ultrasound beam and receiving the reflected echoes, a time duration must be recorded for the series of acoustic reflections. This would be the transit time of the reflections or echoes [2]. The time-of-flight (t) of the pulse reflected from each surface provides the depth information of the sample.

A series of time delays of the pulses from the reflected echoes take place, following interaction with the internals of the sample. The delays relate to the acoustic properties of the material, but mainly to the intrinsic speed of sound of the material and its acoustic impedance [2].

In Fig. 1, one can observe a typical series of echoes against time, and showing relative amplitudes. As it can be noticed from the third echo in the figure, the ultrasonic waves can experience phase inversion, according to the transition type of the acoustic mediums, i.e., from high to low acoustic impedance at the interface, of vice versa. An example interpretation of Fig. 1 could be the following: (1) there are three materials in the structure of the sample, A, B, and C, respectively; (2) there are four interfaces, the first water-to-A interface, the second A-to-B interface, the third B-to-C interface, and the fourth C-to-water interface; (3) the peak of the echoes correspond to the boundaries of the interfaces; (4) the regions in light red, blue, and orange provide a time difference information that can be related to the thicknesses of each corresponding material; (5) the polarity of the echoes indicate that, for example, material A has a higher acoustic impedance than water (potentially harder), and that material C has a lower acoustic impedance than B (potentially softer).

TABLE I. ACOUSTIC-RELATED PROPERTIES OF DIFFERENT MATERIALS [5]

Material	ρ [$\mathrm{kg/m^3}$]	c [$\mathrm{m/s}$]	Z [$\times 10^6\ \mathrm{Ns/m^3}$]
SiC	3,211	13,100	42.1
Sn	7,260	3,320	24.1
Cu	8,960	5,010	44.9
AlN	3,260	10,570	34.46
AlSiC	3,000	8,790	26.4
Al_2O_3	3,987	9,100	32–41
Tungsten	19,250	5,400	104
Gold	19,300	3,316	64
Silver	10,490	3,650	38.28
Nickel	8,900	6,040	53.76
Zinc	7,140	4,210	30.06
Polymer	–	–	2–7
Air	1.293	343	0
Water	997	1,500	1.5
Glass	2,500	6,000	15

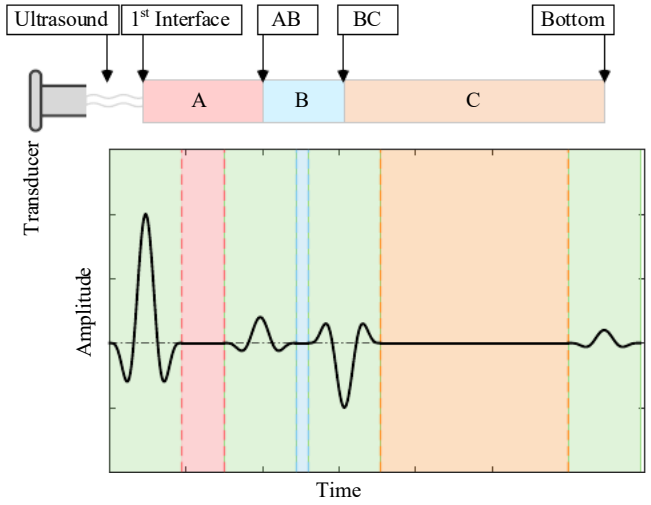

Fig. 1. Example of the A-scan mode of operation, showing ultrasound "echoes" and boundaries

In scanning acoustic microscopy, there are three main modes of operation: A-scan, B-scan, and C-scan. The A-scan provides amplitude, polarity, and time or distance information. In Fig. 1 is shown what an A-scan would represent, and typically, interactive software would display the time-amplitude series by default. On the other hand, the B-

scan provides a cross sectional view through the material which area is parallel to the ultrasonic beam. Conversely, the C-scan provides information of an area that is orthogonal to the ultrasonic beam, recording a single image of the selected layer at a specific depth. Fig. 2 shows a conceptual representation of the concepts of B-scan and C-scan.

While operating in the A-scan mode during preparation, the transducer should be moved in the vertical direction in order to moderate the intensity of the echo related to the layer of interest, before committing to running another type of scan. Whilst the A-scan is the most basic mode, all other modes are just a combination of multiple A-scans, which are then further processed to construct a B-scan or C-scan image. The two scan modes that provide the most meaningful information when inspecting Ag-sintered layers are the A-scan and the C-scan.

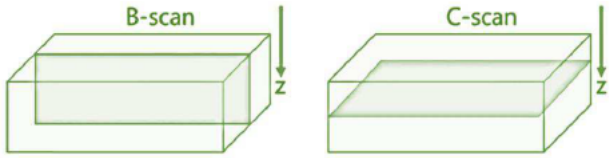

Fig. 2. B-mode and C-mode planes of operation. Adapted from [2]

As mentioned before, an A-scan shows the amplitude along the time, and the relationship between the position of a particular echo in time (t), the travelling distance of the ultrasound (d), and the intrinsic speed of sound of the material (c), is given by:

$$d = \frac{t \times c}{2} \tag{4}$$

There is a trade-off which relates to the resolution versus penetration depth of the sample, normally as the transducer frequency is increased. Theoretically, the resolution (w) can be obtained by means of the following expression:

$$w = \frac{c}{2f \times \mathrm{NA}} \tag{5}$$

Here: c is the speed of sound within the material; f is the frequency of the transducer; NA is the numerical aperture of the transducer. The numerical aperture can then be obtained with the following equation:

$$\mathrm{NA} = \sin\theta \tag{6}$$

However, it is worth mentioning that although the equations (2) and (3) might suggest the ultrasonic beam is either reflected or transmitted, in reality some ultrasonic energy can either be absorbed by the material, or scattered at the interface. Some materials can be quite absorbent of ultrasonic energy, and because at higher frequencies typically less energy can be carried by the ultrasonic beam, higher frequency transducers are most likely to offer less penetration as the ultrasonic beam can be more easily damped or absorbed by the different materials.

This work aims to demonstrate the challenges that must be taken into account when considering the inspection of power electronic modules and other devices, with Ag-sinter technology in mind.

In Section II, we describe the methods, equipment, and instruments utilised for achieving good quality SAM images, and also a description of the experiments is provided. Section III expands on the results obtained through the experiments, providing extensive interpretation of the findings. Here, recommendation techniques on how to achieve the best results are provided when appropriate, the importance of matching and working with different transducers considering different materials in the structure is discussed (including mould compounds), and also X-Ray imaging of selected parts has been conducted in order to compare and highlight the benefits of SAM. Section IV summarises the findings, and concludes the paper.

II. Methodology

A Sonoscan Gen 7 C-SAM microscope is utilised to inspect both soldered and Ag-sintered interfaces between substrates to copper plates, and dies to substrates. The various substrates types to be utilised are AlN/bareCu, and Active Metal Brazed (AMB) AMB-Si_3N_4/Ag-Ni-plated, whilst the dies will be SiC MOSFETs in all cases.

When non-commercial devices are being explored, off-the-shelf Ag-sinter is used, which is adequate for both wet-placing and dry-placing for comparison. Defects will be selectively and purposedly introduced where possible for validation, and large area Ag-sinter attach will be considered. Validation will be conducted using different transducers ranging from 15 to 100 MHz.

TABLE II. Data of the transducers utilised to perform the C-mode SAM scans

Frequency	Focal Length	Diameter [in]	F#	ToF [μs]
15 MHz	0.752	0.50	1.5	25.40
50 MHz	1.000	0.25	4.0	33.87
75 MHz	0.750	0.25	5.0	25.40

For the purposes of calibration and identification of different layers, the following steps must be taken:

1. Position

   The transducer must be moved in the XY dimensions in order to be on top of the sample (ideally the centre, initially). During this step, it must be ensured the transducer is operating correctly, with no air bubbles blocking it. Following this, adjustment in the Z direction must be adjusted, until feedback from the TOF is obtained, guaranteeing the transducer is in a proper operating range.

2. Focus on the first surface

   This can either be done automatically by means of software assistance, or manually, by adjusting the Z-height of the transducer against the surface of interest. The goal is to maximise the echo of interest (in this case the first one, as the first surface is being aimed at). This echo should be constantly monitored or displayed in the A-scan mode. Occasionally, the trigger level must be adjusted in order to discard noise or to get good contrast.

3. Scan the surface of interest

This step allows to verify that the settings are correct, by ensuring a balanced image is being obtained. Otherwise, settings might need adjustment. Although this might sound trivial, at times the user does not know the structure of the inspected sample, and he must ensure meaningful results are being obtained from the equipment.

4. Position the "gate"

   The gate is the term that is typically used to refer to the range of time of the echoes of interest. As discussed in the introduction, echoes reflected from the internal structure present different times in the time series (or A-scan), hence providing depth and thickness information. This means that by adjusting the "gate" or window of interest we are effectively selecting the interface or interfaces to be imaged. Different software tools often offer a multi-gating option, where several windows can be imaged at a time, hence saving time to the user.

5. Re-focus and adjust gain

   By adjusting the Z-height, the transducer penetrates through the structure, effectively focusing more optimally on internal interfaces for which the images will become sharper as it gets closer to the optimal depth of focus. The gain of the transducer can be adjusted as necessary in order to obtain good contrast and balance in the images.

6. Repeat steps 4 – 5 as necessary

When scanning large power modules, a set of fixtures are utilised, which allow for the sample to be scanned from the underside, as a water-jet hits the sample from underneath, so the coupling medium through water is maintained without submerging the part in water.

Apart from SAM, X-Ray imaging is conducted for selected samples. A Dage QUADRA5 X-Ray machine has been used in order to generate images that can be compared to the C-SAM methods utilised.

Since the defect types can be related regardless of the size of the device, or the attaching technology used, we occasionally showcase discrete devices for demonstration purposes, many of which use attaching technologies other than sintering.

In order to demonstrate the capabilities of the C-SAM method, a "story-telling" series of scans are performed, where a 1200 V / 15 A power module with no backplate is scanned to show different layers within the structure.

Following this, a series of C-SAM scans are performed to demonstrate the challenges related to some advanced metallisation types of the substrates. Then, several scans are conducted, this time focused on defect detection, such as voids, cracks and delamination. For this part, both soldered and Ag-sintered devices are utilised, including both discrete devices (TO-247) and custom modules. On the other hand, inspection of large-area Ag-sintered substrates is presented, which also poses its own challenges.

Lastly, a comparison of the performance of different transducers for defect detection is explored. For this part, three 1200 V commercial discrete devices are used (TO-247), all of similar current ratings.

III. Experiments & Results Discussion

A. Extraction of individual layer interfaces

As mentioned in the previous section, when proper attach is achieved within the structure, and good co-planarity is maintained, the different layers within a structure can be identified and separated. This is depicted in Fig. 3, where the sample power module has been inspected to show (a) the copper face of the substrate in the underside; (b) the engraved pattern of the copper on top of the ceramic, where the different components are placed and attached; (c) the attach layer of different components; and (d) the dies.

This is something that would have been practically impossible to achieve if , say, a baseplate with pin-fins had been present.

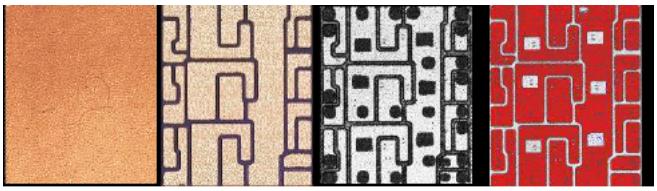

(a) (b) (c) (d)

Fig. 3. C-SAM of a 1200 V / 15A comercial SiC power module. Substrate: AlN/bareCu. Transducer: 75 MHz | 0.750 in | f5.0. The illustration shows: (a) the copper face of the substrate; (b) the engraved pattern of the; (c) the attach layer of components; and (d) the dies

B. Complex surface finish (metallisation) types

Another aspect that must be taken into consideration, is some of the advanced surface finishes or metallisation types with crystallised microstructures that can be used to plate the copper on substrates, with the objectives of preventing copper oxidisation and improving compatibility with other processes, e.g., Ag-sinter. This, however, can blur the sinter layer being inspected and mislead interpretation. In Fig. 4 (a), an example of this type of metallisation is shown. The same figure also shows a SiC die sintered on a substrate with the same surface finish (b), which has a purposedly introduced defect. Fig. 4 (c) depicts a top C-scan which reveals great details of the physical features, shapes, and surfaces, as the metallisation is not obstructing, which is not the case for (d), where the surface finish blurs the image, preventing good levels of detail to be achieved, such as in the case of Fig. 3.

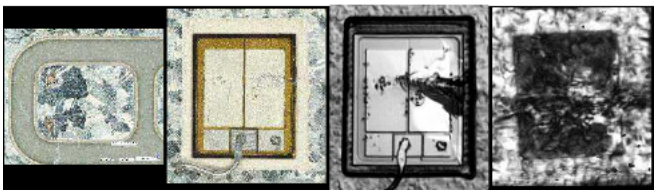

(a) (b) (c) (d)

Fig. 4. Effects of mixed Ag/Ni/Cu plating on defect detection using C-SAM. Showing: (a) surface finish; (b) die sintered on AMB-Si_3N_4; (c) C-SAM image of the top surface of the die showing a purposedly introduced defect; (d) C-SAM image of the die showing distortion due to surface finish

Obviously, complex surface finishes can pose a major challenge when inspecting Ag-sintered layers and other features, as it makes small defects and details undistinguishable from the blur. Most of the time, the user only has access to the internal structure through the back plate

of the module or device (unless, for instance, pin-fins or similar structures are used), hence, this challenge will be present when using similar types of surface finish.

The explanation for this lies in the reflection index of the different elements composing the surface finish metallisation, (e.g., Ag, Cu, Ni, Zn, Au), as reflection index affect the intensity of the echoes at different points, and as a consequence the gradients being imaged vary as well. TABLE III compares the different reflection indexes for the aforementioned materials. The distortion effect caused by the surface finished is magnified significantly when the surface finish is present in both top and bottom sides.

TABLE III. REFLECTION INDEX COMPARISON OF SELECTED MATERIALS, $Z_1 = H_2O$

Material	Z_2 [MNs/m³]	Reflection [p.u.]	Reflection [p.u., normalised]
Zn	30.1	0.82	0.94
Ag	38.3	0.85	0.98
Cu	44.9	0.87	1.00
Ni	53.8	0.89	1.02
Au	64.0	0.91	1.04

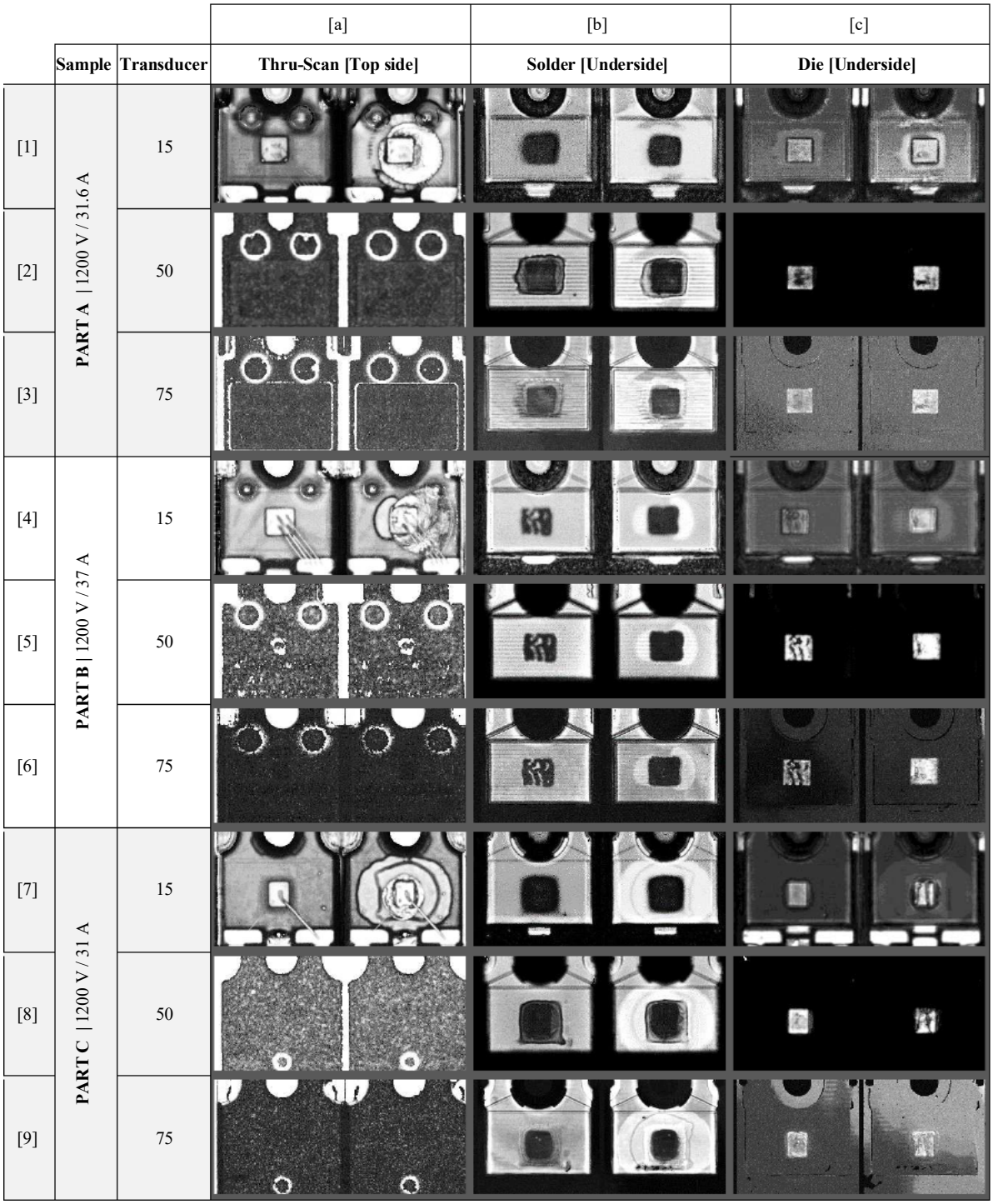

Fig. 5. C-SAM images comparing the effects of different transducers on the image quality, sharpness, and suitability to detect voids, cracks, delamination, and features for three different samples in TO-247 packages, both pristine and failed (short-circuit test). Transducers: 15 MHz | 0.752 in | f1.5; 50 MHz | 1.000 in | f4.0; 75 MHz | 0.750 in | f5.0

C. Defect Detection

As it can be noticed in Fig. 6, a matching transducer must be selected in order to be able to detect defects which are very small. This means, for example, that the small voids shown in Fig. 6 (b) could not have been detected in Fig. 6 (a), which is about 1×1 mm. Furthermore, delamination of the molding compound is shown in (c) for a sample device similar to (a) and (b).

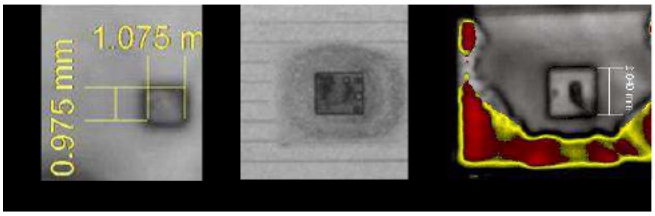

(a) (b) (c)

Fig. 6. Examples of poor focus, small voids, and delamination in TO-247 packaged devices. Showing: (a) die; (b) die; (c) delamination effect. Transducer (a), (c) = 15 MHz | 0.752 in | f1.5; (b) = 75 MHz | 0.750 in | f5.0

A broader comparison of different types of defects (including cracks), is presented in Fig. 5. This figure shows two devices with the same part number for every scan. On the left, a pristine device is shown, whilst next to it to the right, a device with the same part number which has failed a short circuit test is also revealed. For example, the image in position [1][a], shows the sample "PART A" scanned with a 15 MHz transducer, and side by side you have a brand new device (left), and a failed device (right). Referring to the same image, the sample on the left reveals minor delamination on the bottom corners of the surface of the die, even though it is new and unstressed. The sample on the right reveals massive changes in the internals of the moulding compound, as a result of the thermal effects generated during short-circuit test. This particular example is sometimes called "popcorn effect" [6], where delamination is initiated and spread very rapidly.

Another example could be the image [5][c] from Fig. 5, which shows a cracked die on the right hand side. The die shown to the left is masked by voiding area in the solder, which can be verified by looking at the solder layer of the same part in positions [4, 5, 6][b]. It is also notoriously evident that the 75 MHz transducer offers much sharper images of the solder layer, whilst the 50 MHz transducer is more suitable for the detection of cracks.

For all three parts, scans through the structure to visualise the internal structures was only possible using the 15 MHz transducer, as the other two transducers being considered were not able to successfully penetrate through the moulding material whilst scanning from the top side.

Similarly, the different images can be observed to compare and interpret other defect types for all three packages. For instance, the image in position [7][a] shows a minor void in the pristine device, and both voids and delamination in the failed device; [8][c] shows a cracked die on the failed device; [6][b] shows significant voiding in the solder layer.

It is worth mentioning that the different scans most be correlated to accurately distinguish in which layer the defects are really found. Also, the performance of the different transducers to detect the different types of defects is not universal, and greatly depend on the materials and geometries involved.

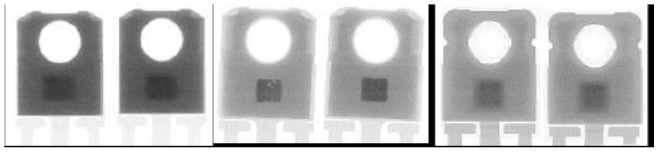

(a) (b) (c)

Fig. 7. X-Ray images of sample parts A, B, and C, respectively | 120 kV 10.8W

The Fig. 7 provides X-Ray images of the same parts provided in Fig. 5. Although very shy features can be recognised (such as the voiding area in the solder layer of the "PART B" to the left, in Fig. 5), the level of detail is no were near to the good results that can be achieved using C-SAM. Also, X-Ray is not effective at all at identifying delamination, cracks, or very small voids in the packages.

The reason for this is that the X-Ray is a transmission imaging technique, and the level of energy that is required to penetrate the copper is the same energy that penetrates through everything in the structure, making other materials negligible.

D. Large area sintering

Another important aspect is the inspection of large areas of sintered materials, such as AMB substrates, or very large dies. Fig. 8 (a) depicts what intuitively appears to be a crack, however, it happens to be a "teardrop" resulting from the moisture in a large area wet-placed substrate. Another example of the same situation is shown in (b). Fig. 8 (c) shows non-uniformity in density of the Ag-layer for a dry-placed substrate, demonstrating a process issue related to dispensing. The same issues related complex surface finishes would also apply, should it have been utilised in the substrates.

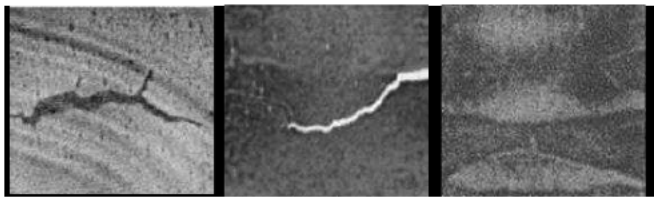

(a) (b) (c)

Fig. 8. Defects in large area Ag-sinter layer of substrates: (a), (b) "teardrop"; (c) non-uniform dispensing (manual)

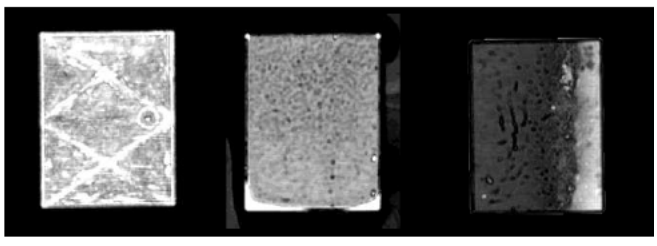

(a) (b) (c)

Fig. 9. Issues related to layer identification, dispensing, and lack of co-planarity. Showing: (a) purposedly introduced pattern on sinter layer; (b) uncovered areas in the bottom corners; (c) non-uniform sintering, related to tooling issues

Fig. 9 (a) demonstrates an important technique which is possible during the design and development process: to

purposedly introduce defects to ensure the right layer is being inspected. While this might sound trivial, it can greatly help set-up and optimise the right settings before massively scanning parts during production. Having done this, Fig. 9 (b) and (c) have been obtained, revealing issues with covering the whole sintering area (dispensing and placing issue), and also the lack of co-planarity, most likely due to problems with the head of the sintering tool.

The final example shows a large area of a commercially available power module. Fig. 10 (a) depicts the solder layer of the substrate to the copper plate. Several voids and poor dispensing in the bottom corners can be seen. Fig. 10 (b) shows the dies on the substrate, which are blurred by the surface finish of the substrate. Also, here some of the voids observed in Fig. 10 (a) can be co-related, as they appear as black dots or patterns. Lastly, Fig. 10 (c) shows an X-Ray image of the same section of the part, for the purposes of comparison.

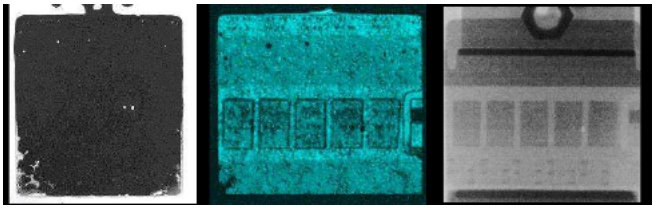

(a) (b) (c)

Fig. 10. C-SAM of an off the shelf SiC power module, 1200 V / 450 A. Showing: (a) solder layer; (b) dies; (c) X-Ray image of the same sample area

IV. Conclusion

Several common challenges and defects related to Ag-sintered components have been captured and demonstrated by means of scanning acoustic microscopy (SAM), following a thorough explanation of the background theory behind SAM, which is not always provided from the practical aspects.

The experiments revealed that C-SAM can be far superior compared to X-Ray when aiming at the attach layers, however, its limitations rely on the geometries involved and the ability of matching transducers that can interact well with the materials and the structures.

Also, it has been proven that SAM can be very effective at identifying all three main types of defects that affect performance and degradation in power electronic modules, and hence it is an ideal tool for inspecting Ag-sintered interfaces.

Complex surface finishes have been presented as a major challenge to the inspection of Ag-sintered layers, mainly because they can obscure the ability to distinguish defects, especially voids and cracks.

Finally, this study has demonstrated that SAM can be extremely effective for the inspection of Ag-sintered layers for both small and large area dies or substrates, and that issues related to the sintering process can be identified, such as dispensing issues or lack of co-planarity of the tooling.

Acknowledgements

The authors wish to acknowledge the support of Andy Walford, George Rowley, and Lewis Stroud, for their technical assistance and knowledgeable discussions at the premises of Custom Interconnect, Ltd.

References

[1] P. Dreher, R. Schmidt, A. Vetter, J. Hepp, A. Karl, and C. J. Brabec, 'Non-destructive imaging of defects in Ag-sinter die attach layers – A comparative study including X-ray, Scanning Acoustic Microscopy and Thermography', *Microelectronics Reliability*, vol. 88–90, no. May, pp. 365–370, 2018, doi: 10.1016/j.microrel.2018.07.121.

[2] H. Yu, 'Scanning acoustic microscopy for material evaluation', *Appl Microsc*, vol. 50, no. 1, 2020, doi: 10.1186/s42649-020-00045-4.

[3] Y. C. Jang, H. E. Kim, A. Schuck, and Y. S. Kim, 'Developed non-destructive verification methods for accelerated temperature cycling of power MOSFETs', *Microelectronics Reliability*, vol. 128, Jan. 2022, doi: 10.1016/j.microrel.2021.114442.

[4] M. Kobayashi, K. Sakai, K. Sumikawa, and O. Kikuchi, 'Signal Processing Method for Scanning-Acoustic-Tomography Defect Detection based on Correlation between Ultrasound Waveforms'.

[5] C. Uhrenfeldt, S. Munk-Nielsen, and S. Bęczkowski, 'Frequency domain scanning acoustic microscopy for power electronics: Physics-based feature identification and selectivity', *Microelectronics Reliability*, vol. 88–90, no. May, pp. 726–732, 2018, doi: 10.1016/j.microrel.2018.07.043.

[6] A. Roy, 'Instrumentation for Studying Real-time Popcorn Effect in Surface Mount Packages during Solder Reflow', *International Journal of Electronics Science and Engineering*, vol. 7, pp. 1126–1130, 2013.